Machine Learning on Greenest Pixels for Crop Mapping

Ziheng Sun, Liping Di, Hui Fang

zsun@gmu.edu; ldi@gmu.edu (corresponding author); hfang1288@gmail.com

Center for Spatial Information Science and Systems

George Mason University

4087 University Dr STE 3100

Fairfax, VA, USA, 22030

Abstract: Crop fields are full of uncertainties due to the complexity of the environment, seeds, climate, market, and farmers. It is a common phenomenon that the crops in neighbor fields are in different growing stages, e.g., the corns in one field are already dented but just emerged in another neighbor field. The phenomenon results in remote sensing images that are non-ideal for producing crop maps as the crops are in different phases across the fields. For instance, July is the best month for monitoring soybeans but bad for winter wheat. Most of the wheat fields are already harvested in July and appear like fallow fields on satellite images. This paper proposes a customized classification approach based on greenest pixels (GP) to enhance the quality of the satellite images for mapping. The greenest pixels are got by calculating the largest NDVI (Normalized Difference Vegetation Index) values of every pixel from all the captured images each year. In the process, we filtered the bad quality pixels like clouds, ice, snow, shadow, etc. A filtering step is added to distinguish the non-vegetation and vegetation pixels first. The overall workflow uses state-of-art remote sensing classification techniques. Machine learning (ML) algorithms like KNN, Gaussian Naïve Bayes, Decision Tree, AdaBoost, Random Forest, SVM, and Neural Networks were used simultaneously to evaluate the approach. The study area is located on the farms of Nebraska. They used satellite imagery includes Landsat 8 surface reflectance products. The ground truth data comes from field surveys, roadside samples, and USDA (United States Department of Agriculture) crop maps. Google Earth Engine was used to accelerate the data preprocessing. We tested all the ML models on two sets of experiments: GP and non-GP. In each set, the training has only one-year data (2013) and the testing uses the rest years (2014-2018). The results show that the proposed GP-based approach can significantly improve the classification precision by ~20% (from ~70% to ~85%) on average. This research proves that greenest pixels have large potential and should be considered as the major input data in the crop mappings in the future.

Keywords: greenest pixel; machine learning; land cover; remote sensing; image classification.

1. Introduction

Remote sensing plays a big role in agriculture monitoring today. Satellites, drones, airplanes take thousands of images about farm fields every day [1-5]. A lot of useful information is hidden in these images. Via these images, people can monitor the recent progress of crops, analyze the impacts of disasters, and study the vegetation phenology [6,7]. To reveal the contained information and make them easy to read, scientists produce many thematic maps regarding various application purposes. For instance, agricultural drought maps are generated to guide the irrigation [7-9]. Vegetation health maps are derived to guide the use of chemicals to boost the yields and protect the crops from disease, weeds, infestation, etc [10,11]. The crop distribution map is normally produced annually to show the crop types growing on the fields in that

41   year [12]. Due to the low cost and high availability of remote sensing images, remote sensing image
42   classification is now the major method to produce in-time and large-scale agricultural thematic maps [13].
43   The common classification techniques can be categorized into two types: unsupervised classification
44   and supervised classification [14]. Thematic classification tasks like crop distribution mapping should use
45   supervised classification [15]. To assist the supervised classification on a large scale, a tremendous amount
46   of ground truth data points is required to train the models and validate the results. However, the cost of
47   collecting ground truth data is much higher than remote sensing data at present, which is one of the major
48   bottleneck problems in crop mapping. USDA (United States Department of Agriculture) has devoted long-
49   term efforts to survey the crop fields every year and collected a complete systematic set of ground
50   measurements by their field offices. Use that data, USDA NASS (National Agricultural Statistics Service)
51   produces Cropland Data Layer (CDL), annual crop maps of continental United States at the resolution of
52   30 meters by classifying the imagery of Landsat and some other satellites [16,17]. See5, a renowned decision
53   tree software, is used to carry out the classification for CDL [18]. CDL owns a very high accuracy that
54   ranges from 82% to 95%. Some large farm areas could even reach to 97% [1,17]. Recent new research
55   shows that applying new supervised classification could improve the accuracy further while reducing the
56   dependence on ground truth data by creating reusable classification models. Many papers highlighted ML
57   models could increase the accuracy and reusability significantly [12,19-22].
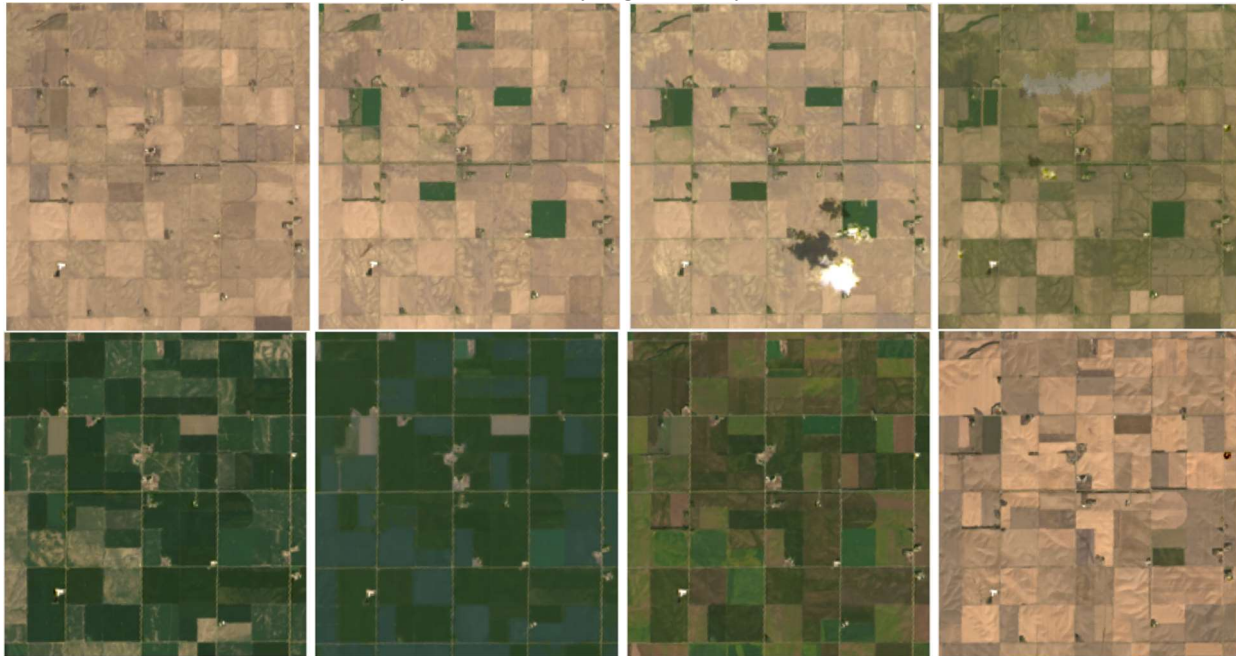
58
59
60   Figure 1. The raw true-color Landsat images (top row from left to right: 2018-04-05, 2018-05-07, 2018-
61   05-23, 2018-06-08; bottom row from left to right: 2018-07-10, 2018-08-11, 2018-09-12, 2018-11-15)
62   Besides ground data, the selection of remote sensing images is another challenge in improving map
63   quality. The phenology of various crop types has huge differences, which results in that not all the remote
64   sensing images are suitable for classification. Fig. 1 shows the Landsat true-color images [23] of the same
65   area on different days in 2018. This area is located at the heart of Nebraska, a major corn/soybean state in
66   the nation [6]. The image of April 5 has no green fields, indicating that no crops are planted or not emerging
67   yet. This image doesn't contain any information on crops. In the images on May 7 and 23, several alfalfa
68   fields become green as they are planted early and grow fast. In the June 8 image, cornfields start to green
69   up while some of the alfalfa fields have been cut for the first time (alfalfa field turns light green). In the
70   July 10 image, corn has entered the black layer stage, while soybeans also become visible. On August 11,
71   corn and soybean have reached full maturity and are ready for harvesting. Alfalfa was harvested for another

72 time and turns light green again. On September 12, most corn fields were harvested, and alfalfa grows up
73 again. In the November 15 image, all the fields returned to idle like the first image of April 5. The first four
74 images and the last two images are not suitable to identify corn and soybeans but good for recognizing
75 alfalfa and field ridges. The revisiting period of the same place of every satellite differs every year and so
76 do the crop phenological milestones, which are greatly influenced by the farmer's decisions and
77 environment. Due to these uncertainties, searching and selecting suitable remote sensing images suitable
78 for classification takes a lot of manual efforts and is labor-intensive to scale up to a large scale and charges
79 a higher cost on consumers to get high-resolution crop maps.

80   To address these challenges, this paper proposes a novel approach using greenest images and machine
81 learning (ML) models in producing crop maps. Greenest images are calculated by extracting the greenest
82 pixels from all the captured images in one year. The greenness is measured by NDVI (normalized difference
83 vegetation index) [24]. In other words, the pixels with the highest NDVI values are considered as the
84 greenest pixels. The pixels in the greenest image should all be the greenest of the year. Classic ML models
85 are created to take the greenest images as inputs and output a thematic map of crop types. The resulting
86 map is a raster image, in which the pixel values correspond to crop categories. For instance, 1 represents
87 corn, and 5 represents soybean. Fig. 2 shows a comparison between original true-color Landsat images,
88 greenest images, and thematic crop maps in 2018. It is clear that all the crop fields in the greenest image
89 are green and covered by crops, unlike the original Landsat images always including some idle fields. The
90 thematic crop map renders different land cover types with various colors for better readability. In the CDL
91 hierarchy, there are more than 100 crop types.
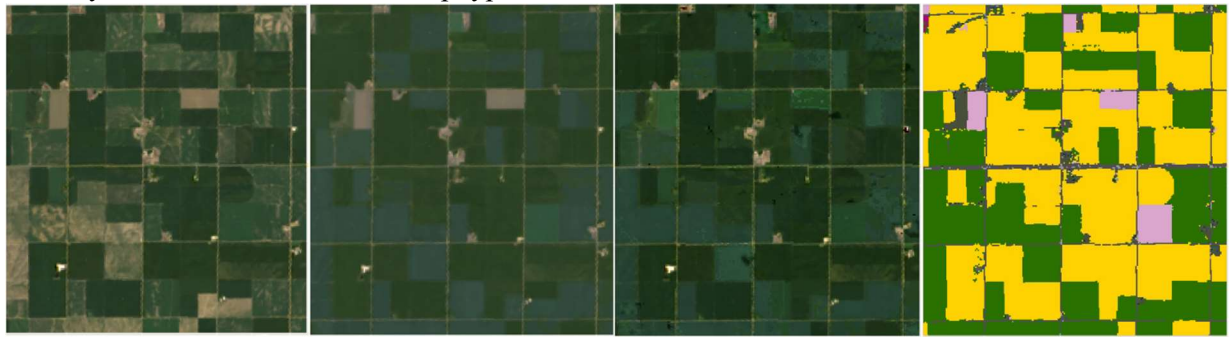
92
93 Figure 2. From left to right: 07-10-2018, 08-11-2018, Greenest Image of 2018 and CDL of 2018 (yellow:
94   corn; green: soybean; pink: alfalfa; black: roads)

95   In this work, a new workflow streamlining the preparation and feeding of greenest images into ML
96 models is built and experimented. The workflow translates the ML model results to crop maps which are
97 ready for stakeholders to use. The whole workflow involves dozens of tools, resources, and libraries, and
98 requires better management to improve efficiency. The study area chooses a farm located in the heart of
99 Nebraska and the data sources are Landsat 8. The images are preprocessed to become consumable arrays
100 in ML models. Classic ML models including KNN, Gaussian Naïve Bayes, AdaBoost, Decision Tree, SVM,
101 Random Forest, and Multilayer Perceptron, are all tested to validate the superiority of the GP approach.
102 The ML models extract the high-level features from the images to identify and recognize the crops. Random
103 Forest and Multilayer Perceptron have been proven to be more accurate and generalizable than the other
104 classification models regarding both major and minor crops. The trained models are proven to be reusable
105 on future images to automatically generate crop maps without needs for collecting new ground truth or
106 retraining.

107   The remainder of this paper is organized as follows. Section 2 gives the background and motivation of
108 this work. Section 3 introduces the study area and the used datasets. In Section 4, deep learning is briefly
109 introduced as the existing state-of-art work. Section 5 describes the proposed GP-based approach. The
110 experiment and results are described in Section 6 and Section 7 evaluates the performance of the approach

111 by comparing it to other existing approaches. Section 8 concludes the work and gives the work items in the
112 future.

113 **2. Background**

114 2.1 The Role of Farm Maps in Decision Making

115   Smallholder farmers are sitting on the front line of agricultural decision making. They are farmers that
116 have more than half of farm work done by family members, cooperative members or neighbors. Decision
117 making is central to farm management. Each decision has an impact on the farm and the farm household.
118 Even deciding to do nothing is a decision and has an impact. The more a farmer is aware of the decision-
119 making processes that affect farm and household, the more sustainable the farm will be and the more likely
120 it will be profitable and sustainable. Farm decisions are closely tied to decisions made in the household.
121   The most characteristic aspects of farming operations are the changes that continuously occur, and the
122 lack of knowledge concerning conditions that affect farm businesses. Market prices, the knowledge of
123 smallholder farmers, techniques, weather, health, and governmental arrangements change all the time.
124 Throughout the agriculture history, farmers had to make decisions based only upon observation and
125 recollection. Both sources are not precise, but it was the best data available [25].
126   As scientific methods were introduced, farmers could employ research-derived recommendations to
127 improve production efficiency. Digital technologies are changing the routine of farmers in making their
128 daily decisions. The evolution of those capabilities offers significant benefits for farmers and the entire food
129 supply industry[1]. Farmers have long desired to link measures of outcomes and management actions in
130 farming. Advanced technologies like remote sensing and sensor web give farmers the ability to routinely
131 capture and exploit data to get their desired information. The crop distribution map is an important member
132 of the desired data. Farmers need to get an overview of what other farmers are growing and how many acres
133 are covered by the same crop over the entire region. The information would greatly help them make an
134 economic-wise choice on choosing crops to increase their household income.
135   Other thematic farm maps will identify areas on the farm that are vulnerable to water contamination,
136 and practices that may contribute to water pollution. The base map of the farm should show all farm fields,
137 the farmstead and barnyard area, associated use areas, wetlands, and forests. Another value of a farm map
138 is for future planning or to best utilize their property. A farm map can also identify soil types and other
139 characteristics, such as slope, that can be useful in making decisions like grazing plans and crop rotations.
140 A map can be helpful when selecting compost or manure storage areas. It can also play an important role
141 in emergency planning or responding. [2]

142 2.2 Challenges and Opportunities

143   Cutting-edge techniques have been utilized in farmland mapping for a long time. Satellite remote
144 sensing is a low cost and reliable way and has been used in the land survey for many years. The remote
145 sensing data is mostly available free and easy to access via web services. Recently, NASA and NOAA have
146 worked with giant tech companies to migrate their big datasets to the commercial clouds that have better
147 scalability and stability for data retrieval. Cloud-native services provide big data processing capabilities
148 that are never seen before, such as Google Earth Engine (GEE). This latest development in satellites and
149 cloud computing has made it convenient to produce agriculture maps in an efficient and economical manner.
150 With the development of intelligent farming devices such as autonomous tractors, remotely monitoring
151 farmland and operating devices to farm efficiently is a big wish of the humankind for the next generation
152 of agriculture. Remote sensing is a key component playing the eye-in-the-sky role in this ambitious vision.

---

[1] https://farmdocdaily.illinois.edu/2020/03/evidence-data-and-farmer-decision-making.html
[2] https://njaes.rutgers.edu/fs1189/

153 It provides critical information about the crops in the field and transfers the information to decision making
154 parties to develop and apply solutions or operations.

155 **3. Data and Study Area**

156 3.1 Study Area

157   The study area is within the central region of Nebraska, one of the major corn-belt states. The crops
158 include soybeans, and corn, alfalfa, and some winter wheat. In 2018, the ten leading commodities for cash
159 receipts in Nebraska are cattle and calves, corn, soybeans, hogs, wheat, dairy products (milk), misc. crops,
160 hay, chicken eggs, and potatoes. Among them, corn is Nebraska's most important crop, with much of it
161 going to feed cattle and hogs. The state had 45,900 farms and ranches during 2018 and the average operation
162 consisted of 980 acres (397 ha). The landscape of Nebraska has a 4,584 feet elevation difference, and the
163 average annual precipitation decreases by one inch every 25 miles from east to west. The agricultural
164 industry in Nebraska shows a diverse change from one side to the other.

165 3.2 Data Sources

166 (1) Landsat 8

167   Landsat 8 is the latest in-orbit satellite of the Landsat program and was launched in 2013 [23]. The
168 satellite has two major sensors onboard: Operational Land Images (OLI) and the Thermal Infrared Sensor
169 (TIRS). It circles the Earth every 99 minutes and has a 16-day repeat cycle for any location on the Earth. It
170 acquires about 740 scenes a day on the Worldwide Reference System-2 (WRS-2) path/row system. The
171 mostly used bands come from OLI include nine bands at 30-meter resolution. The band range is kept
172 consistent with the bands of old TM/ETM sensors carried by previous Landsat satellites.

173 (2) Cropland Data Layer (CDL)

174   CDL is a georeferenced raster crop map of the U.S. at a spatial resolution of 30 meters. It is derived by
175 classifying satellite imagery using reliable classification algorithms and the massive amount of ground truth
176 data collected by the United States Department of Agriculture (USDA) National Agricultural Statistics
177 Service (NASS). It is released yearly and normally published in next February. The accuracy in the crop
178 fields ranges from 85% to 95%. The data is available for the lower 48 states since 2008. Before that, only
179 a few states are available. Due to its high quality, it has been used in many major researches related to
180 agriculture by both academia and industries.

181 (3) Roadside Survey

182   The ground truth data of USDA, Common Land Unit (CLU), is not in the public domain [26]. To
183 validate our classification results, we collected ground observations via very high-resolution images, field
184 surveys, and road trips. Many people in the U.S. enjoy identifying and observing farms and farm activity
185 while on a road trip. We made several trips to Nebraska and drive a big circle from Omaha to Ogallala and
186 drive back via Norfolk. The trips occurred in July and we took 1,095 photo samples in total showing the
187 growing crops. We processed all the photos and translate them into a collection of ground truth polygons
188 as shown in Fig. 3. This work extracts and utilizes those samples located in the study area.

189

190   Figure 3. Roadside Survey (yellow: corn; green: soybean)

191   **4. Greenest Pixel**
192   NDVI is a measure of the greenness of land surface and associated objects. The values range from 0 to
193   1. Using greenness is a great way to deal with the discontinuities between Landsat paths, in the median
194   pixel composite due to the differences in phenology as a result of images in adjacent paths being collected
195   at different times. One way to minimize that is to set pixel values in the composite from roughly the same
196   phenological stage, for example, the time of maximum greenest of plants (when the leaves are on and
197   photosynthetically active). The entire time series is examined and the pixel with the maximum value in the
198   NDVI band is set as the composite value. Vegetated areas all appear green because NDVI is highest when
199   the vegetation in the pixel is photosynthetically active. By defining the max greenness by the maximum
200   NDVI, we can use the mosaic method to make a composite in which each pixel contains the maximum
201   NDVI pixel from the collection. The result will be the greenest pixel composite. Fig 2 shows a list of
202   monthly greenest pixel composite images, which are calculated for all the images captured in each month.
203   Indeed, compared to the median composite, the greenest pixel composite is much greener. In the greenest
204   images, there are fewer clouds or bad quality pixels. The images are clean and bright. In the greenest images,
205   the changes in crops over the time series are revealed very explicitly.
206   The re-composited, cloud-free, greenest Landsat products should be able to provide consistent spatial
207   and temporal comparisons of global vegetation conditions which are used to monitor the Earth's
208   photosynthetic vegetation activity for phonological, change detection, and biophysical interpretations. The
209   composites are calculated from cloud-free and atmospherically corrected gridded surface reflectance. It
210   requires a series of multi-temporal geo-referenced satellite data to be processed into NDVI images. Each
211   pixel will examine its NDVI value and only the highest value is retained for each pixel. After all the pixels
212   have been evaluated, the resulting image is known as the greenest image.

213

214
215   Figure 4. Monthly greenest true-color images in 2018 (top from left to right: April, May, June, July;
216   bottom from left to right: August, September, October, November)

217   The Landsat time-series dataset could be represented by the following definition:

218    $I = \{ f_{y,d,lon,lat,b} \mid y \in [2013, 2019], d \in [1, 366], lon \in [-180, 180], lat \in [-90, 90], b \in [0, 11] \}$

219   The set I represents the whole Landsat 8 dataset from 2013 to 2019. The function $f_{y,d,lon,lat,b}$ returns
220   observation values. y stands for year, d is the Julian day of the year, lon and lat represent longitude and
221   latitude, and b means the 12 bands from the Landsat Level 1 surface reflectance products. The set of
222   greenest pixels is defined as:

223    $GP = \{F_{x,y,b} \mid y \in [2013, 2019], b \in [0, 11], x \in I, x' \in I, Y_x = Y_{x'}, LON_x = LON_{x'}, LAT_x = LAT_{x'}, D_x$
224    $\neq D_{x'}, and\ NDVI_x > NDVI_{x'}\}$

225   where the y is the year, b is the bands; x and x' are two Landsat pixels; the observation year Y, latitude
226   (LAT) and longitude (LON) of x and x' are the same; the observation day D of x and x' are different; the
227   NDVI of x is greater than the NDVI of any qualified x'. The NDVI equation is:

228    $$NDVI_x = \frac{F_{x,5} - F_{x,4}}{F_{x,5} + F_{x,4}}, x \in I$$

229   For Landsat 8, NDVI is equal to the difference between band 5 and band 4 divided by the sum of the two.

230   **5. Machine Learning Models**
231   In this section, several classic ML models are introduced. They have been studied for a long time and
232   used in many projects. These models were tested on the GP images for comparison to find out the
233   algorithms with the best performance.

234   5.1 KNN
235   KNN, short for K nearest neighbor, is an entry-level machine learning algorithm [27]. For every pixel
236   in the imagery, it aims to find the K samples from the ground measurements which have the most similar
237   features to the pixel. In the K samples, the class with the most votes will claim the pixel.

238   5.2 Naïve Bayes
239   Naïve Bayes is a family of fast probabilistic algorithms and suitable for processing a large amount of
240   data [28]. It takes advantage of Bayes' Theorem of probability for prediction of the unknown class under
241   the assumption that the features have strong (naïve) independence among them. It calculates the probability
242   of each class for a given object, and then output the class with the highest probability. Gaussian Naïve
243   Bayes (Gaussian NB) extends the Naïve Bayes to real-valued attributes by assuming a gaussian distribution.
244   First, we can calculate the mean and standard deviation of input values (x) for each class to summarize the
245   distribution. In addition to the probabilities for each class, the mean and standard deviations for each input
246   variable of each class must be stored as well. To make predictions, the Gaussian probability density function
247   (PDF) is used. The new input for the variable is plugged into the function, and in return, the gaussian PDF
248   will provide an estimate of the probability of that new input value for that class.

249    $$PDF(x, mean, sd) = (\frac{1}{\sqrt{2 \times PI} \times sd}) \times e^{-\frac{x - mea^2}{2 \times sd^2}}$$

250   where $PDF(x, mean, sd)$ is the Gaussian PDF, mean and sd are the mean and standard deviation, PI is the
251   numerical constant. We can then plug in the probabilities into the equation above to make predictions with
252   real-valued inputs [29].

253   5.3 AdaBoost
254   AdaBoost [30] is a classification algorithm by fitting a sequence of weak learners (models that are just
255   slightly better than random guessing) on repeatedly modified versions of the data. The predictions from all
256   of them are then combined through a weighted majority vote to get the final prediction. Each data

257 modification is called a boosting iteration which consists of applying weights $w_1, w_2, ..., w_n$ to each of the
258 training samples. Initially, the weights are all set to $1/N$ (N is the total number of samples), so the first step
259 will simply train a weak learner on the original data. In the following steps, the weights will be individually
260 modified, and the learning algorithm is reapplied to the reweighted data. At each step, those incorrectly
261 predicted samples will have their weights increased, whereas the weights are decreased for those correctly
262 predicted. After a few iterations, samples difficult to predict will get higher and higher influence. The
263 classifier will be forced to concentrate on the examples that are missed by the previous iterations in the
264 sequence[3].

265 5.4 Random Forest
266   Random forest [31] is an improved algorithm of the basic decision tree. Instead of only one tree, the
267 random forest will create many trees. Instead of just simply averaging the results of the trees (a forest), RF
268 model uses two key ideas to make it random: (1) random sampling of training data points when building
269 trees; (2) random subsets of features considered when splitting nodes. To classify a new object from an
270 input vector, put the input vector down each of the trees in the forest. Each tree gives a classification to vote
271 for one class. The forest chooses the classification having the most votes. When the training set for the
272 current tree is drawn by sampling with replacement, about one-third of the cases are left out of the sample.
273 This OOB (out-of-bag) data is used to get a running unbiased estimate of the classification error as trees
274 are added to the forest. It is also used to get estimates of variable importance. After each tree is built, all of
275 the data are run down the tree, and proximities are computed for each pair of cases. If two cases occupy the
276 same terminal node, their proximity is increased by one. At the end of the run, the proximities are
277 normalized by dividing by the number of trees. Proximities are used in replacing missing data, locating
278 outliers, and producing illuminating low-dimensional views of the data. Because of the out-of-bag estimate
279 internally, there is no need for cross-validation or a separate test set to get an unbiased estimate of the test
280 set error.

281   Random forest is much better to avoid overfitting than one single decision tree. Overfitting means that
282 the model not only learns the actual relationships in the training data, but also the noises. The noise part
283 will make the trained model yield a very poor performance on new data.

284 5.5 Support Vector Machine (SVM)
285   SVM [32] is inspired by the idea to find a hyperplane that best divides a dataset into two classes. Support
286 vectors are the data points nearest to the hyperplane. If some support vectors are removed, the hyperplane
287 will move too. So the support vectors are considered as the critical elements of a data set. The distance
288 between the hyperplane and the nearest data point from either set is known as the margin. The goal is to
289 choose a hyperplane with the greatest possible margin between the hyperplane and any point within the
290 training set, giving a greater chance of new data being classified correctly. In other words, for linearly
291 separable patterns, SVM could create optimal hyperplane to distinguish them. For the patterns that are not
292 linearly separable, SVM uses the Kernel function to transform original data and map them into a new space.
293 In that space, it would be easier to create the hyperplane.

294 5.6 Multilayer Perceptron (MLP)
295   MLP [33] is one basic type of neural network which has multiple hidden layers (perceptron) beside an
296 input layer to receive the signal and an output layer that makes decisions or predictions about the input. The
297 arbitrary number of hidden layers that are the true computational engine of the MLP. They are trained on a
298 strict set of input-output pairs and learn to model the correlation between the inputs and outputs. Training
299 involves adjusting the parameters, or the weights and biases, of the model to minimize error.

---

[3] https://scikit-learn.org/stable/modules/ensemble.html#adaboost

300 Backpropagation is used to make those weigh and bias adjustments relative to the error, and the error itself
301 can be measured in a variety of ways. One usual way is by the root mean squared error.

302 MLP belongs to the family of feedforward neural networks which have two major constant activities:
303 forward and back. In the forward pass, the signal flow moves from the input layer through the hidden layers
304 to the output layer, and the decision of the output layer is measured against the ground truth labels to
305 calculate the errors. In the backward pass, using backpropagation and the chain rule of calculus, partial
306 derivatives of the error function are back-propagated through the hidden layers. The differentiation
307 produces a gradient along which the parameters can be adjusted to make the result of the next attempts
308 closer to the error minimum. The forward and back processes keep going until the error is lowered under a
309 threshold or the error doesn't change by several consecutive loops.

310 **6. Methods**

311 6.1 General description

312 This work proposed an approach to integrate the preprocessing steps of greenest pixels into the
313 established machine learning workflow. The approach was designed to map crops including both food crops
314 and cash crops. The training data for machine learning comes from ground-measured data and refined CDL.
315 For the non-cropland area, the land cover labels of NLCD are assumed correct and reused in this approach.
316 The classification is pixel-based using the multiband values of Landsat 8 as inputs and a label value as
317 outputs. The classification module can switch among the algorithms described in Section 5.

318 6.2 GP-ML workflow

319 This workflow, named GP-ML, includes four main steps: 1) get greenest pixel products and identify
320 potential crop fields; 2) assign a crop type using the CDL, roadside photos and remote sensing images; 3)
321 perform classification using the mentioned machine learning models and the prepared training dataset; and
322 4) refine the incorrect initial crop types in those edge areas of crop fields, and integrate the CDL product,
323 non-crop land cover, refined ground samples, and the ML generated results to produce the final crop map
324 products. These four steps are further described as follows.

325 6.2.1 Identify Potential Crop Fields

326 To identify potential crop fields, we first compiled the areas where the Landsat imagery fully covered
327 in the growing season and retrieve all the available images. NDVI is calculated for every Landsat image
328 which filtered clouds and shadows based on the quality band. We extracted the pixels whose NDVI values
329 are larger than 0.4. The threshold is set to be 0.4 based on empirical experiences and numerous experiments
330 by referring to ground photos and samples. The pixels with NDVI larger than 0.4 have a very high chance
331 to be at least 60% vegetation area. However, it is hard to distinguish the forests from crops simply using
332 NDVI. We used the cultivated mask layer from USDA to further extract the pixels to get the crop fields.

333 6.2.2 Image Classification

334 The greenest pixels of the recognized crop fields and the corresponding crop types are used as the
335 training dataset for machine learning classification. The combined training data, along with all the Landsat
336 images of 2015 are used as input data into the machine learning classifiers to train the models. The trained
337 model will be used to produce crop maps for the next few years, e.g., 2015, 2016, 2017, 2018. During the
338 model training, the connections between the Landsat observations and the crops growing in the fields will
339 be learned and used to establish the rules (Random Forest, Decision Tree), create hyperplanes (SVM) and
340 tune the weights (MLP). For the other classifiers, the encoding of crop types uses a continuous list of
341 integers each of which represents a land cover type and all the null classes in the CDL hierarchy are cleaned.
342 For the MLP, one-hot encoding is used to encode the crop types into arrays instead of a particular integer.
343 The classification is mainly based on the spectral information of the pixels. Not much shape and texture

344 information are utilized in the process. The experiments on the two sets of experimental data will reveal the
345 benefits of greenest pixels and the better ML models for classification on greenest pixels.

346 6.2.3 Accuracy assessment

347 Confusion matrix-based metrics are used to evaluate the performance of GP-ML and compare the
348 machine learning models, evaluating its improvements over the non-GP approach. The used metrics include
349 precision, recall, and F-1. The assessment focused on the cropland areas since the goal of the method was
350 to produce crop field maps. Two sets of sample points were selected: the first set was used to evaluate the
351 overall accuracy of the method to map crop fields based on greenest pixels; the second set was used to
352 assess the accuracy of the non-greenest pixels. To draw the first set of sample points, random sampling is
353 used by extracting all the areas which have NDVI values larger than 0.4. 100 points could provide a
354 reasonably good accuracy estimate. For each pixel, a reference point of crop types was derived by visual
355 interpretation from roadside photos and high-resolution images provided by USDA NAIP (National Aerial
356 Imagery Program).

357 6.2.4 Post-refinement Processing

358 We refined the results by correcting errors such as the pixels which are classified as crops which
359 contrast to the ground truth and the inappropriate crop labels in the edge areas of the crop fields and the
360 water shallow region. The cultivated layer from USDA may exclude some crop fields or include some non-
361 crop fields. To correct this, we visually identified some missing fields by comparing the crop maps from
362 machine learning models with high-resolution satellite images. After we confirm there is a crop field, we
363 will manually change the mask and rerun the model to generate a crop type for the pixel. For those pixels
364 in wetlands or edge areas, we will determine by the neighbor pixels. If over 60% of neighbor pixels are the
365 same crops, we will assign the same crop type to the pixel.

366 **7. Results**

367 7.1 Image Processing

368 Google Earth Engine is used to collect all the intersected Landsat scenes with the study area and 100
369 roadside images were processed to create 6 greenest pixel images from 2013 to 2018. The quality of the
370 greenest images is significantly improved and the missing pixels are much less and the cloud and shadow
371 areas in the original Landsat scenes are replaced or filled using the greenest observation. Jupyter notebook
372 is used as the developer environment. Scikit-learn library is used to train machine learning models. The
373 training of each model takes about 2 hours. The SVM and Random Forest takes more time than other
374 models. All the models are trained and tested on the same training dataset. We use the images from 2013
375 as the training samples and test on the images from the next five years (as shown in Table 1). Only one-
376 year data is used for training because we want to shorten the training time cost and emphasize the generality
377 test of the models. All the models are applied to both the greenest pixel and raw pixel training datasets. The
378 pixels are filtered by cloud and vegetation masks before they are fed into the ML models for testing. The
379 predicted results are ensembled back into images corresponding to their input pixel locations.

380 Table 1. Experiment Settings

Experiment	Train	Test	Methods
Greenest Pixel	2013 Yearly Greenest Pixels	2014 – 2018	Random Forest
			SVM
			Gaussian Naïve Bayes
			Decision Tree
			AdaBoost
			KNN
			MLP
Raw Landsat Pixels	2013	2014 – 2018	Random Forest

	LC08_L1TP_031031_20130726		SVM
	LC08_L1TP_031031_20130827		Gaussian Naïve Bayes
			Decision Tree
			AdaBoost
			KNN
			MLP

381 7.2 Comparison of GP and non-GP
382   The results of GP and non-GP in the same year from 2014 to 2018 are compared. In Fig. 5, the top two
383 rows show the non-GP results of Aug 14, 2014, and the bottom two rows show the GP results of 2014. The
384 differences are clear. In general, the GP models outperformed the non-GP models with a very large margin.
385   For the raw Landsat image, SVM and AdaBoost classified almost all the pixels to cornfields. In the
386 non-GP results of RF and DT, the soybean fields are misclassified to corn, while cornfields are misclassified
387 to soybean fields. Gaussian NB recognized most of the field edges and classify all the pixels into cornfields.
388 KNN generates a similar result to the Random Forest but shows some scattered soybean pixels in the middle
389 of cornfields. MLP result agrees with the Random Forest result on those soybean fields which are wrongly
390 categorized into cornfields. This experiment shows that for raw Landsat images, there is no big
391 improvement by only changing the classification models. The same mistaken pixels can be found in most
392 models' results. Overall, training data is the key to improve the accuracy and generality of the ML models.
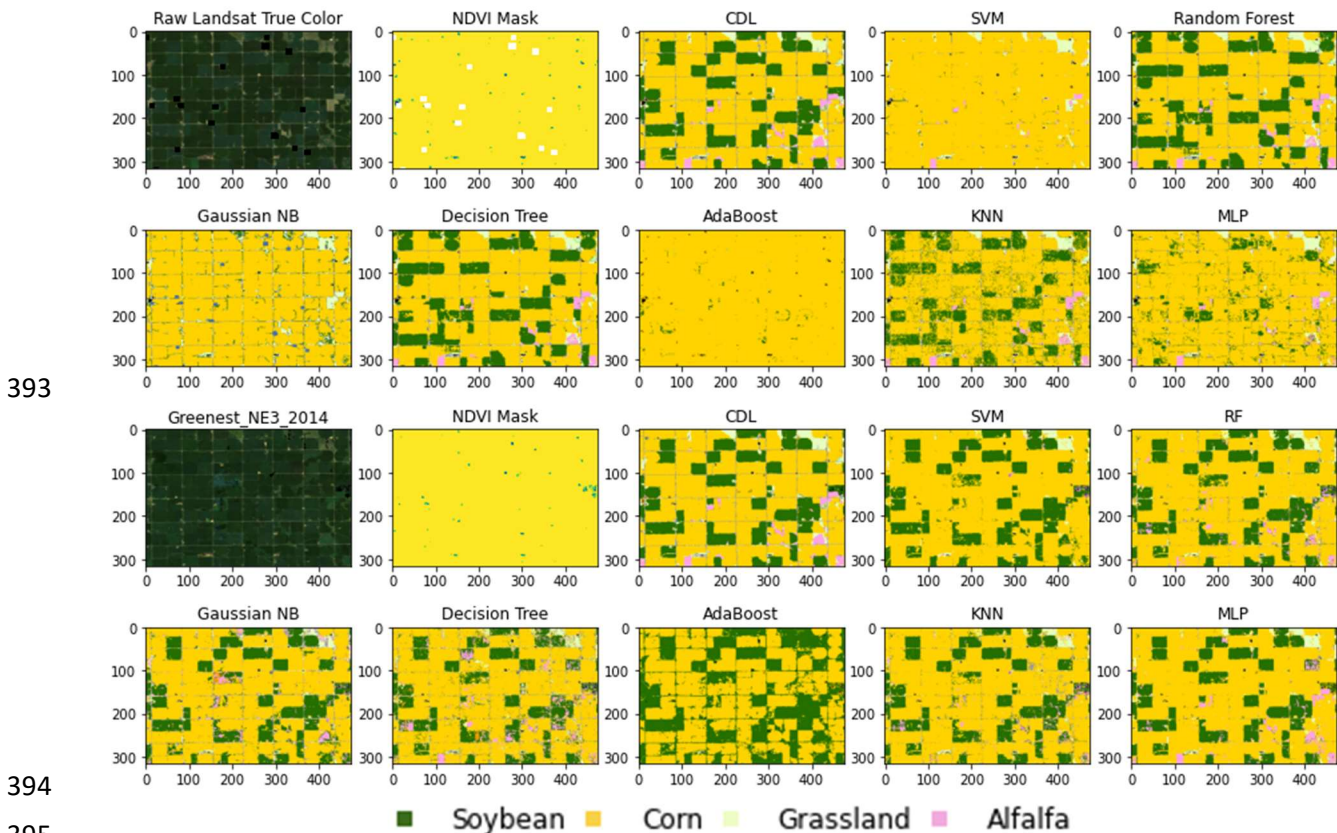
393

394

395

396 Figure 5. Comparison between 2014 non-GP (1st and 2nd rows) and 2014 GP (3rd and 4th rows) classification results
397 (top row from left to right: true-color Landsat image, NDVI mask, CDL, SVM, Random Forest; bottom
398 row from left to right: Gaussian NB, Decision Tree, AdaBoost, KNN, MLP)

399   For the greenest image, all the models generate some reasonably accurate results, with most corn and
400 soybean fields correctly classified. The NDVI mask shows that the greenest pixel image has much fewer
401 blank pixels than the original Landsat image. The grassland regions are greener in the true color images.

402   The alfalfa and grassland are separated very well. The results of SVM, RF, KNN, and MLP agree on the
403   corn and soybean fields. The difference is mainly on some scattered alfalfa pixels. From the perspective of
404   alfalfa, the MLP result has the most identical classification to the CDL. SVM, RF, and KNN all classified
405   some corn pixels into alfalfa. Decision Tree result has noisy texture in the cornfields with soybean pixels
406   all over. Gaussian NB again has the best results on field edges. Gaussian NB did a good judgment, except
407   that one small soybean field in the middle of the image is classified into alfalfa by Gaussian NB. AdaBoost
408   has the poorest prediction in this experiment. It did recognize most of the soybean and cornfields, however,
409   neglect the short-sampled classes like grassland and alfalfa.

410   After observing the two experiments, it is clear that every ML model did a better prediction on the
411   greenest pixel image than the raw Landsat image. It proves the quality of the training data plays a key role
412   in crop classification. The conclusion could be supported by quantitative metrics of accuracy. The measures
413   of both experiments on the test datasets of four years (2015-2018) are plotted in Fig. 6. Three common
414   indicators are evaluated against the result pixels and the ground truth. The precision of the same models is
415   higher than 76% on GP but less than 70% on non-GP in 2015. In the 2015 GP experiment, RF has the most
416   consistent accuracy with the second-highest precision (only after MLP) and the highest recall and F1 score
417   (88%). In the non-GP experiment on the Landsat image of July 16, 2015, Gaussian NB is the most accurate
418   model on all three metrics. In the 2016 results, the GP-based RF achieves as high as 92% in precision and
419   94% in recall. KNN, MLP, and SVM also did very well on precision and recall. Decision and AdaBoost
420   are not as good as the other four. However, on the non-GP, SVM performs the best with 72% precision,
421   75% recall, and 67% F1. KNN has the lowest precision and F1 and Decision Tree has the lowest recall. In
422   the 2017 result, GP-trained SVM outperforms the other methods with a very consistent value (89%) on the
423   three indicators. The decision tree is the model with the worst result. For the non-GP in 2017, AdaBoost
424   has the best performance with 74% precision, 79% recall, and 74% F1, and KNN has the poorest measures.
425   In the 2018 GP result, RF again claims the first place with 90% precision, 90% F1 and 93% recall. MLP
426   and SVM did the same best. DT and AdaBoost are the two models with the worse predictions. In the non-
427   GP 2018 result, Gaussian NB is the best model and the AdaBoost is the worst.

428   The experiment results show that the models have very unstable performances on the non-GP data. It
429   is found to be very inconsistent over the four years on the best and worst models. In every year, the non-
430   GP-trained models perform very poorly (50% ~ 75% in precision) on new data (trained on 2013 and tested
431   on the subsequent years), which reflects the generality of the trained models is bad. However, the same
432   models trained on GP have very solid and relatively steady accuracy (about 80% ~ 95%). The model
433   performs better on GP than non-GP in every case. The results have the most consistent precision and recall.
434   The two metrics differ dramatically in the non-GP results, which indicates that the non-GP-trained models
435   either underfit on the majority or overfit on the minority. In conclusion, the GP training dataset could
436   significantly improve the accuracy of the result crop maps on both major crops and minor crops. The models
437   trained on GP have much better generality and accuracy than those trained on non-GP.
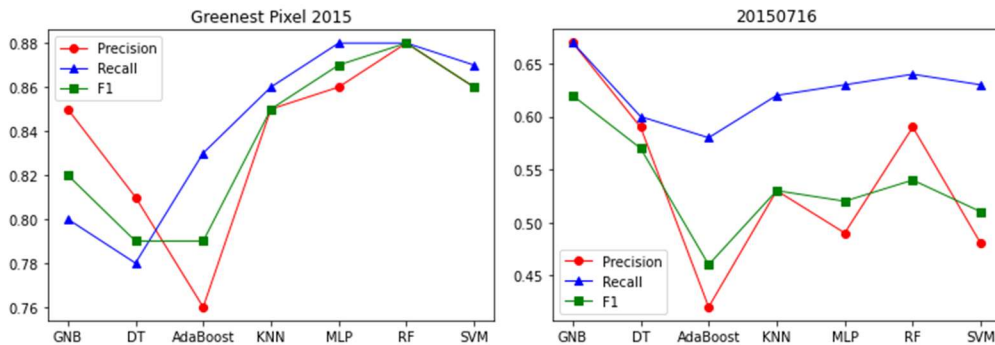
438
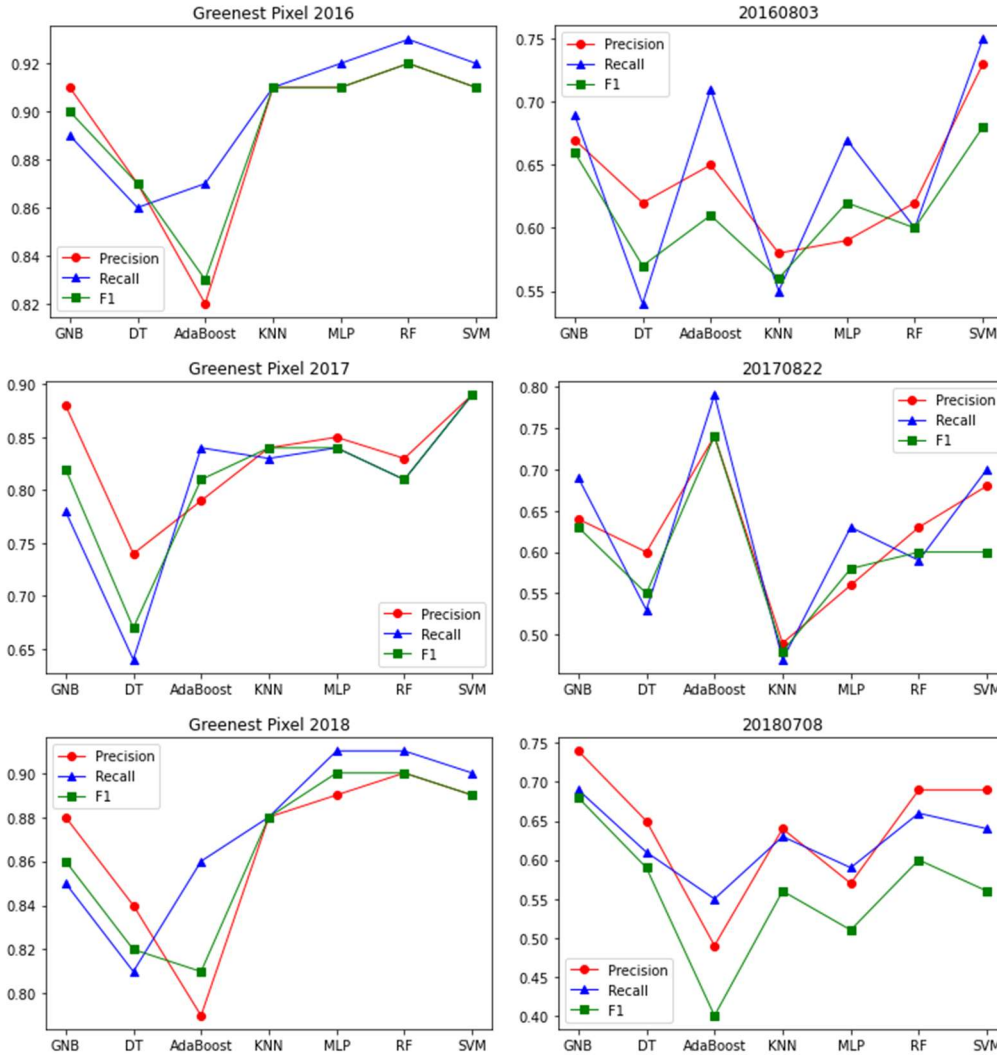
439
440
441
442   Figure 6. Accuracy Comparison of ML models on greenest pixels (left) and raw Landsat pixels (right)

443   7.3 Comparison of ML Algorithms

444   To find the best algorithm for GP, the results of the GP-trained models in all four years (as shown in
445   Fig. 7) are thoroughly studied. Every year, the ML models display a similar pattern in their judgments.
446   SVM can accurately identify soybeans, corns, and grassland, but cannot recognize alfalfa and field edges.
447   SVM misclassified most alfalfa pixels into soybeans. Gaussian NB makes big mistakes in some big soybean
448   fields by classifying them into alfalfa fields. Corn and grasslands are correct. The results of single Decision
449   Tree are very poor with vague and dirty texture and many pixels with classes that don't exist in the region.
450   Single Decision Tree is not recommended for this purpose. AdaBoost did a good job of outlining the field
451   borders. It made the right judgment on the major crops but completely ignored the minor crops. The pixels
452   of grassland and alfalfa are assigned to either corn or soybeans (mostly). KNN outputs a very similar result
453   to the RF and MLP, except for some error spots of soybeans in the middle of cornfields. The KNN result is
454   less smooth and consistent compared to RF and MLP.

455   The results of RF and MLP are better than other models. models accurately recognize the soybean, corn
456   and grassland fields. It is hard to tell which one of the two is the best. RF delineates the field borders more
457   clearly than MLP while MLP gives better prediction on alfalfa than RF. In other words, if the borders are
458   important target information, RF is recommended; if minor crops like alfalfa are required information, MLP
459   would be the better choice.
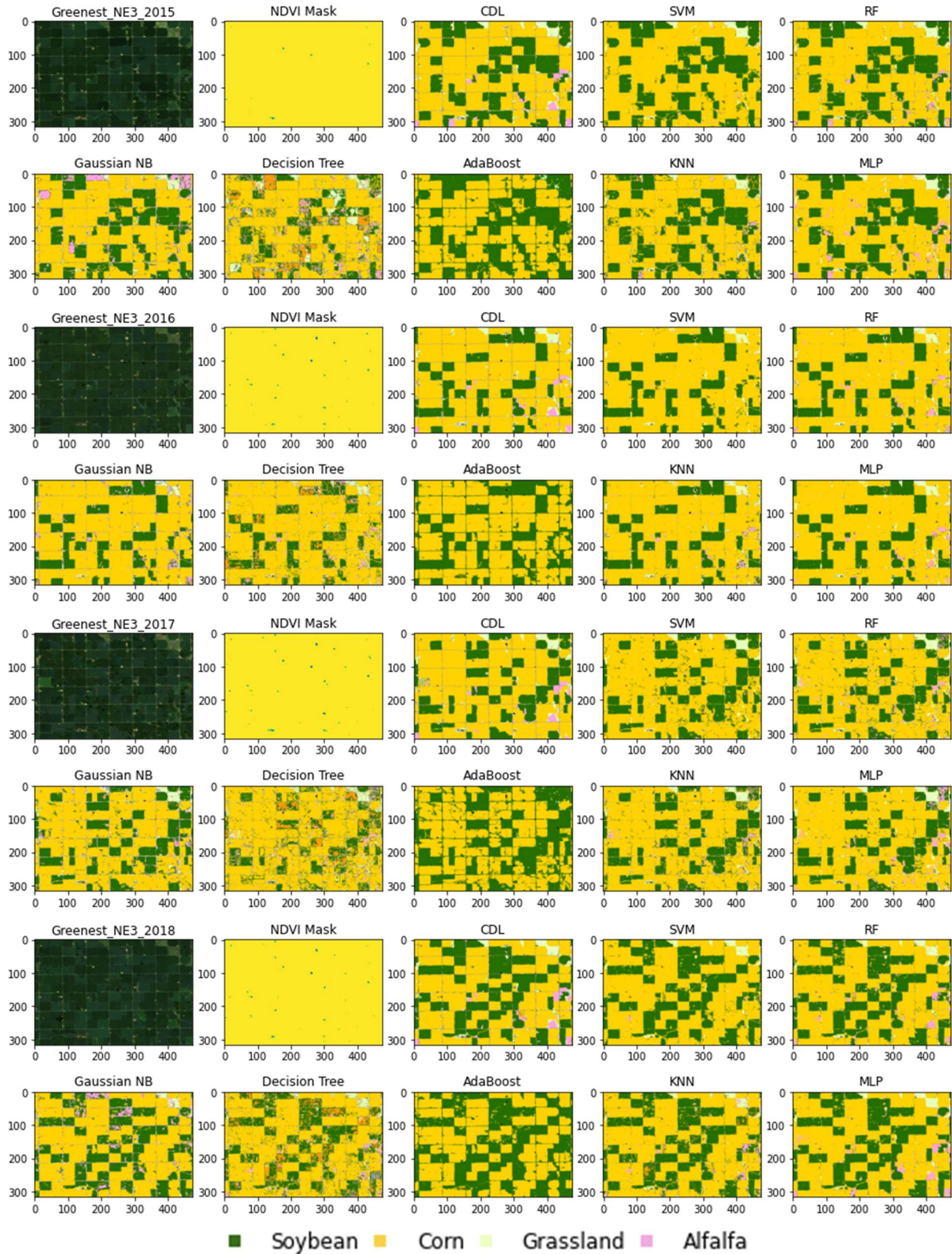
Figure 7. Comparison of the Algorithms on greenest pixels (trained on 2015, tested on 2013, 2014, 2016, 2017, 2018)

8. Discussion

8.1 **Reliability**: will the GP-trained models always beat the non-GP models?

Based on the experiment results, the GP-trained ML models outperformed the non-GP-trained models. To rule out the concerns on coincidences, we did another test in the region shown in Fig. 1 and got the same results (GP better than non-GP). The reason is that in the GP the crops and non-crop vegetation are all in their greenest phases, which narrows down the characteristics of the crops into a limited feature space. Therefore, using the GP training dataset the ML models don't need to make wild guesses on which phase the crops are in and require fewer rules or features to distinguish the crops. In other words, the GP training dataset makes the job of ML models much easier than the non-GP training dataset. The superiority of GP-trained models over non-GP models is not coincidental and should be reproducible all the time.

8.2 **Generality**: will the best ML models for this region always be the top choice for any other regions?

The comparison of ML models in image classification has been studied for a very long time. As one of the common techniques for improvements, hyperparameter tuning could greatly alter the performance of the ML models and bring a lot of uncertainties to the comparison. In this study, we didn't do much tuning on the hyperparameters. All the parameters use their default values provided by the ML library. If the hyperparameter tuning is taken into consideration, the answer to the generality question would be a NO. However, if taking hyperparameter tuning off the table, the answer would be certainly a YES. Without tuning parameters, the Random Forest and Multilayer Perceptron will produce better results for all the regions out of the six listed ML models.

8.3 **Scalability**: will the same quality results be achieved if the region is extended to a larger scale?

This question needs more experiments on bigger datasets to answer. At this point, we could only anticipate from the theoretic perspective. The quality of training data would still be key to scale the trained models to be applied in a larger scope. If the samples used for training are less biased and cover most of the unique statuses of the objects, the trained model would obtain more capability to deal with the upcoming new pixels from new images of various regions. The bias of training data is not only about the regions, but also in the classes. Naturally, some crops have more samples (e.g., corn and soybean) while others have fewer occurrences (e.g., lentils). Each class should have a certain minimum number of samples in the training data to ensure the minority crops could be distinguished. In the GP approach, the variety of regions have relatively fewer impacts on the results as the same crop of different regions has very similar spectral characteristics during its greenest stage (assuming the climate of those regions is similar). Overall, better scalability will be achieved with better training data.

9. Conclusion

This paper proposes a novel approach using greenest images and ML algorithms in producing crop maps. Greenest images are calculated by extracting the greenest pixel value from all the captured images in one year. The greenness is measured by NDVI (normalized difference vegetation index). The pixels with the highest NDVI values are considered as the greenest pixels. The pixels in the greenest image should all be the greenest. An approach is created to generated and take the greenest images as inputs and output a semantic map of crop types. The map is a raster image, in which the pixel values correspond to crop categories. A new workflow streamlining the preparation and feeding of greenest images into ML models is built and experimented. The workflow will translate the ML model results in crop maps which are ready for stakeholders to use. The whole workflow involves dozens of tools, resources, and libraries, and requires better management to improve efficiency. The study area chooses a farm located in the heart of Nebraska and the data sources are Landsat and USDA NASS CDL. The images are preprocessed to become consumable arrays in ML models. The training among the hidden layers of ML models will extract the high-level features to identify and recognize the crops. RF and MLP have been proven to be more accurate

512 and robust than the other classification models. The trained model is supposed to be reusable on future
513 images to automatically generate crop maps without needs for collecting new ground truth or retraining.
514 The results show that the GP-trained ML models outperformed the non-GP-trained ML models with a very
515 large margin.

516   In the future, more experiments on a bigger training dataset will be conducted to verify the superiority
517 of the GP-based approach in larger regions. More advanced ML models such as convolutional neural
518 networks and recurrent neural networks will be tested against GP to further improve the accuracy. The
519 readiness of the GP-trained model to produce official crop maps from remote sensing images will be
520 evaluated and carried out in Nebraska in our next step of research.

521

522 **Reference**

523

524 1. Sun, Z.; Di, L.; Fang, H. Using long short-term memory recurrent neural network in land cover
525   classification on Landsat and Cropland data layer time series. *International Journal of Remote*
526   *Sensing* **2018**, *40*, 593-614.
527 2. Pinter Jr, P.J.; Hatfield, J.L.; Schepers, J.S.; Barnes, E.M.; Moran, M.S.; Daughtry, C.S.; Upchurch,
528   D.R. Remote sensing for crop management. *Photogrammetric Engineering & Remote Sensing*
529   **2003**, *69*, 647-664.
530 3. Adão, T.; Hruška, J.; Pádua, L.; Bessa, J.; Peres, E.; Morais, R.; Sousa, J. Hyperspectral imaging: A
531   review on UAV-based sensors, data processing and applications for agriculture and forestry.
532   *Remote Sensing* **2017**, *9*, 1110.
533 4. Sun, J.; Di, L.; Sun, Z.; Shen, Y.; Lai, Z. County-Level Soybean Yield Prediction Using Deep CNN-
534   LSTM Model. *Sensors* **2019**, *19*, 4363.
535 5. Sun, Z.; Di, L.; Fang, H.; Burgess, A.B.; Singh, N. Deep Learning Cyberinfrastructure for Crop
536   Semantic Segmentation. In Proceedings of AGU Fall Meeting 2019.
537 6. Sun, Z. Automatically Recognize Crops from Landsat by U-Net, Keras and Tensorflow. Availabe
538   online: https://medium.com/artificial-intelligence-in-geoscience/automatically-recognize-crops-
539   from-landsat-by-u-net-keras-and-tensorflow-7c5f4f666231 (accessed on 1/26/2020).
540 7. Zhong, S.; Xu, Z.; Sun, Z.; Yu, E.; Guo, L.; Di, L. Global vegetative drought trend and variability
541   analysis from long-term remotely sensed data. In Proceedings of 2019 8th International
542   Conference on Agro-Geoinformatics (Agro-Geoinformatics); pp. 1-6.
543 8. Sun, Z.; Di, L.; Zhang, C.; Fang, H.; Yu, E.; Lin, L.; Tan, X.; Guo, L.; Chen, Z.; Yue, P. Establish
544   cyberinfrastructure to facilitate agricultural drought monitoring. In Proceedings of Agro-
545   Geoinformatics, 2017 6th International Conference on; pp. 1-4.
546 9. Sun, Z.; Di, L.; Zhang, C.; Fang, H.; Yu, E.; Lin, L.; Tang, J.; Tan, X.; Liu, Z.; Jiang, L. Building robust
547   geospatial web services for agricultural information extraction and sharing. In Proceedings of
548   Agro-Geoinformatics, 2017 6th International Conference on; pp. 1-4.
549 10. Sun, Z.; Peng, C.; Deng, M.; Chen, A.; Yue, P.; Fang, H.; Di, L. Automation of Customized and
550   Near-Real-Time Vegetation Condition Index Generation Through Cyberinfrastructure-Based
551   Geoprocessing Workflows. *Selected Topics in Applied Earth Observations and Remote Sensing,*
552   *IEEE Journal of* **2014**, *7*, 4512-4522, doi:10.1109/jstars.2014.2377248.
553 11. Yang, Z.; Di, L.; Yu, G.; Chen, Z. Vegetation condition indices for crop vegetation condition
554   monitoring. In Proceedings of Geoscience and Remote Sensing Symposium (IGARSS), 2011 IEEE
555   International; pp. 3534-3537.

556 12. Xiong, J.; Thenkabail, P.S.; Gumma, M.K.; Teluguntla, P.; Poehnelt, J.; Congalton, R.G.; Yadav, K.;
557   Thau, D. Automated cropland mapping of continental Africa using Google Earth Engine cloud
558   computing. *ISPRS Journal of Photogrammetry and Remote Sensing* **2017**, *126*, 225-244.
559 13. Moran, M.S.; Inoue, Y.; Barnes, E. Opportunities and limitations for image-based remote sensing
560   in precision crop management. *Remote Sensing of Environment* **1997**, *61*, 319-346.
561 14. Banman, C. Supervised and Unsupervised Land Use Classification. Availabe online:
562   http://academic.emporia.edu/aberjame/student/banman5/perry3.html (accessed on
563 15. Sun, Z.; Fang, H.; Di, L.; Yue, P.; Tan, X.; Bai, Y. Developing a web-based system for supervised
564   classification of remote sensing images. *GeoInformatica* **2016**, 1-21.
565 16. Johnson, D.M.; Mueller, R. The 2009 cropland data layer. *Photogramm. Eng. Remote Sens* **2010**,
566   *76*, 1201-1205.
567 17. Boryan, C.; Yang, Z.; Mueller, R.; Craig, M. Monitoring US agriculture: the US department of
568   agriculture, national agricultural statistics service, cropland data layer program. *Geocarto*
569   *International* **2011**, *26*, 341-358.
570 18. Quinlan, J.R. See5. *URL: http: www. rulequest. com/see5-info. html* **1997**.
571 19. Duro, D.C.; Franklin, S.E.; Dubé, M.G. A comparison of pixel-based and object-based image
572   analysis with selected machine learning algorithms for the classification of agricultural
573   landscapes using SPOT-5 HRG imagery. *Remote Sensing of Environment* **2012**, *118*, 259-272,
574   doi:http://dx.doi.org/10.1016/j.rse.2011.11.020.
575 20. Waldner, F.; Canto, G.S.; Defourny, P. Automated annual cropland mapping using knowledge-
576   based temporal features. *ISPRS Journal of Photogrammetry and Remote Sensing* **2015**, *110*, 1-
577   13.
578 21. Fritz, S.; See, L.; McCallum, I.; You, L.; Bun, A.; Moltchanova, E.; Duerauer, M.; Albrecht, F.; Schill,
579   C.; Perger, C. Mapping global cropland and field size. *Global change biology* **2015**, *21*, 1980-
580   1992.
581 22. Gao, F.; Anderson, M.C.; Zhang, X.; Yang, Z.; Alfieri, J.G.; Kustas, W.P.; Mueller, R.; Johnson,
582   D.M.; Prueger, J.H. Toward mapping crop progress at field scales through fusion of Landsat and
583   MODIS imagery. *Remote Sensing of Environment* **2017**, *188*, 9-25.
584 23. Roy, D.P.; Wulder, M.; Loveland, T.; Woodcock, C.; Allen, R.; Anderson, M.; Helder, D.; Irons, J.;
585   Johnson, D.; Kennedy, R. Landsat-8: Science and product vision for terrestrial global change
586   research. *Remote Sensing of Environment* **2014**, *145*, 154-172.
587 24. EOS. NDVI FAQ: All You Need to Know About NDVI. Availabe online: https://eos.com/blog/ndvi-
588   faq-all-you-need-to-know-about-ndvi/ (accessed on 2020.03.16).
589 25. Johnson, G.L.; Haver, C.B. Decision-making principles in farm management. **1953**.
590 26. USDA, F. Common land unit. *FSA Handbook, 8-CM* **1998**.
591 27. Dudani, S.A. The distance-weighted k-nearest-neighbor rule. *IEEE Transactions on Systems, Man,*
592   *and Cybernetics* **1976**, 325-327.
593 28. Chan, T.F.; Golub, G.H.; LeVeque, R.J. Updating formulae and a pairwise algorithm for computing
594   sample variances. In Proceedings of COMPSTAT 1982 5th Symposium held at Toulouse 1982; pp.
595   30-41.
596 29. Brownlee, J. Naive Bayes for Machine Learning. Availabe online:
597   https://machinelearningmastery.com/naive-bayes-for-machine-learning/ (accessed on
598   4.13.2020).
599 30. Hastie, T.; Rosset, S.; Zhu, J.; Zou, H. Multi-class adaboost. *Statistics and its Interface* **2009**, *2*,
600   349-360.
601 31. Breiman, L. Random forests. *Machine learning* **2001**, *45*, 5-32.
602 32. Cortes, C.; Vapnik, V. Support-vector networks. *Machine learning* **1995**, *20*, 273-297.

603   33.   SUTER, B.W. The multilayer perceptron as an approximation to a Bayes optimal discriminant
604   function. *IEEE Transactions on Neural Networks* **1990**, *1*, 291.

605